



Article

Synthesis of Highly Photoluminescent All-Inorganic CsPbX₃ Nanocrystals via Interfacial Anion Exchange Reactions

Zongtao Li ¹ , Cunjiang Song ¹, Longshi Rao ^{1,2,*} , Hanguang Lu ¹, Caiman Yan ¹, Kai Cao ¹, Xinrui Ding ¹, Binhai Yu ¹ and Yong Tang ¹

¹ Engineering Research Centre of Green Manufacturing for Energy-Saving and New-Energy Technology, School of Mechanical and Automotive Engineering, South China University of Technology, Guangzhou 510640, China; meztli@scut.edu.cn (Z.L.); scj1778407030@126.com (C.S.); guyuexuan1999@foxmail.com (H.L.); chamenyan@163.com (C.Y.); 201821002410@mail.scut.edu.cn (K.C.); dingxr@scut.edu.cn (X.D.); bhaiyu@yeah.net (B.Y.); ytang@scut.edu.cn (Y.T.)

² College of Engineering, Shantou University, Shantou 515063, China

* Correspondence: memerls@mail.scut.edu.cn

Received: 26 July 2019; Accepted: 8 September 2019; Published: 11 September 2019



Abstract: All-inorganic cesium lead halide perovskite CsPbX₃ (X = Cl, Br, I) nanocrystals (NCs) have attracted significant attention owing to their fascinating electronic and optical properties. However, researchers still face challenges to achieve highly stable and photoluminescent CsPbX₃ NCs at room temperature by the direct-synthesis method. Herein, we synthesize CsPbX₃ NCs by a facile and environmentally friendly method, which uses an aqueous solution of metal halides to react with Cs₄PbBr₆ NCs via interfacial anion exchange reactions and without applying any pretreatment. This method produces monodisperse and air-stable CsPbX₃ NCs with tunable spectra covering the entire visible range, narrow photoluminescence emission bandwidth, and high photoluminescence quantum yield (PL QY, 80%). In addition, the chemical transformation mechanism between Cs₄PbBr₆ NCs and CsPbX₃ NCs was investigated. The Cs₄PbBr₆ NCs were converted to CsPbBr₃ NCs first by stripping CsBr, and then, the as-prepared CsPbBr₃ NCs reacted with metal halides to form CsPbX₃ NCs. This work takes advantage of the chemical transformation mechanism of Cs₄PbBr₆ NCs and provides an efficient and environmentally friendly way to synthesize CsPbX₃ NCs.

Keywords: Cs₄PbBr₆ NCs; CsPbX₃ NCs; interfacial anion exchange; chemical transformation

1. Introduction

In recent years, all-inorganic cesium lead halide perovskite CsPbX₃ (X = Cl, Br, and I) nanocrystals (NCs) have attracted a lot of attention due to their excellent properties, such as high photoluminescence (PL) quantum yield (QY), broad wavelength coverage, narrow PL emission bandwidth, and low trap state density [1–4]. These outstanding properties of CsPbX₃ NCs distinguish them from traditional semiconductor NCs and make them promising candidates for various optoelectronic applications, including solar cells [5], lasers [6], photodetectors [7], and light emitting diodes (LEDs) [8].

To date, many methods have been developed for the synthesis of CsPbX₃ NCs, such as hot-injection [9], solvothermal synthesis [10], post-treatment [11], ultrasonication [12], and mechanochemistry [13,14]. However, researchers still face challenges to achieve highly stable and photoluminescent CsPbX₃ NCs at room temperature by the direct-synthesis method. In addition to studying various direct synthesis methods, the chemical transformation of pre-synthesized NCs has drawn researchers' attention in synthesizing CsPbX₃ NCs because they allow for the precise control of the NCs and enable the synthesis of materials with different morphologies and sizes,

such as nanowires and nanorods that are difficult to obtain directly [15,16]. Recently, the chemical transformation between non-luminescent Cs_4PbX_6 and luminescent CsPbX_3 has sparked researchers' interest. For example, the Akkerman group [17] treated pre-synthesized Cs_4PbX_6 NCs with excess PbX_2 to synthesize green fluorescent CsPbX_3 NCs. The Jing group [18] reported highly luminescent CsPbBr_3 nanorods (NRs) through chemical transformation from Cs_4PbBr_6 NCs and tuned PL emission of the NRs over the full visible range through a halide anion-exchange reaction using hot-injection. During these processes, anion exchange is a common strategy used to modify the chemical composition of as-prepared NCs and regulate their spectrum. However, most chemical transformation anion exchange processes use oleylamine-X or PbX_2 as anion sources, which require inert conditions, high temperatures, and pre-treated precursors [19]. For example, anion sources, such as PbX_2 need to be dissolved in octadecene (ODE) first and then a is added, such as oleic acid or oleylamine, to dissolve the halogen ions. Moreover, in order to obtain highly stable and PL QY NCs, inert conditions are required during the anion exchange process. These anion exchange methods are limited to the direct mixing of solid halogen ions with perovskite solutions, which not only requires a cumbersome dissolution process but also brings in a large number of non-luminescence materials during the anion exchange process.

Ion transport across the interface between two immiscible liquids is a fundamental study in catalysis and electrochemistry, namely, different ions can be transferred through the interface of two incompatible solvent interfaces. Herein, we report a novel interfacial anion exchange route in the chemical transformation of Cs_4PbBr_6 to CsPbX_3 on the n-hexane/water interface. Taking advantage of ion transport across the interface between two immiscible liquids, we can easily synthesize highly stable and PL QY CsPbX_3 NCs at room temperature. By using different metal halides, the band-gap energy and PL spectra were readily tuned over the entire visible spectral region. Differing from the mostly reported chemical transformation used anion sources, the metal halides are dissolved in deionized water due to their high solubility in water. This process does not need any complicated pretreatment, such as heating in a vacuum or adding oleic acid and oleylamine to dissolve the halide source, which not only improves synthetic efficiency and product purity but also lowers the production cost. In addition, the chemical transformation mechanism between Cs_4PbBr_6 NCs and CsPbX_3 NCs was investigated. We further demonstrated the potential applications of the perovskite NCs in white LED (WLEDs) by combining the green luminescent CsPbBr_3 NCs with red luminescent CdSe NCs and a blue GaN LED chip, showing an encompassing 125% color gamut of the National Television System Committee (NTSC, 1913) standard.

2. Materials and Methods

2.1. Chemicals and Materials

Cesium carbonate (Cs_2CO_3 , 99.99%), lead bromide (PbBr_2 , 99.99%), 1-octadecene (ODE, 90%), oleic acid (OA, 90%), and oleylamine (OAm, 90%) were purchased from Sigma-Aldrich Co. (St. Louis, MO, USA). N-hexane, methyl acetate, and poly (methyl methacrylate) (PMMA) were purchased from Shanghai Aladdin Biochemical Technology Co. (Shanghai, China). Transparent silicone resin (OE-6650A and B) was purchased from Dow Corning Co. (Midland, MI, USA). All chemicals were used as received without any further purification.

2.2. Preparation of Cesium-Oleate Solution

A total of 0.16 g Cs_2CO_3 (0.49 mmol), 1.0 mL OA and 16 mL ODE were loaded into a 30 mL flask, dried for 30 min at 120 °C under N_2 , and then heated to 150 °C until all Cs_2CO_3 reacted with OA to form a cesium-oleate solution.

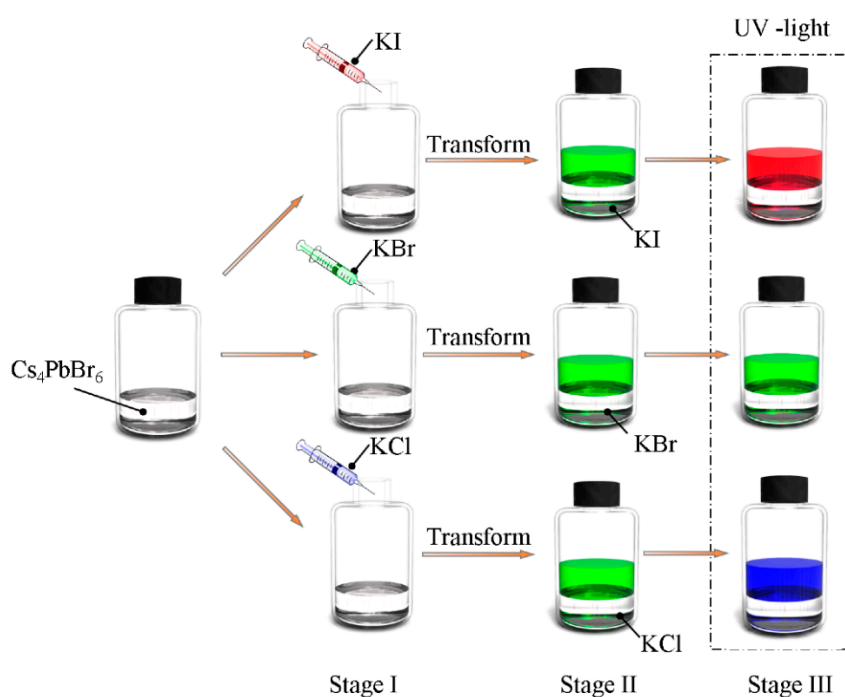
2.3. Preparation of Cs_4PbX_6 NCs

In a typical synthesis of Cs_4PbBr_6 NCs, 1.0 mL OAm, 1.0 mL OA, 10 mL ODE, and 0.2 mmol PbBr_2 were loaded into a 25 mL three-neck flask and dried under vacuum for 30 min. The reaction

system was heated to 140 °C. Then, hot (~150 °C) Cs-oleate solution (4.4 mL in ODE, the molar ratio of Cs-oleate and PbBr₂ was 1.35:1, prepared as described above) was rapidly injected into the PbBr₂ solution. Seven seconds later, the mixture was immediately cooled with an ice-water bath.

2.4. Interfacial Anion Exchange Reactions

The anion exchange process on the interface of n-hexane/KX aqueous solution is shown in Scheme 1. The reaction was conducted under ambient condition. In a typical interfacial anion exchange process to prepare CsPbI₃, 3.0 mL Cs₄PbBr₆ n-hexane dispersion was added into a 10 mL glass bottle. The original Cs₄PbBr₆ solution is colorless, as shown in Scheme 1-Stage I. Then, 3.0 mL KI aqueous solution (0.5 M) was injected quickly, the color of the upper Cs₄PbBr₆ n-hexane dispersion was changed from colorless to green rapidly under UV light irradiation, as shown in Scheme 1-Stage II. After 24 h, the color of supernatant gradually turned yellow, orange, and eventually red, as shown in Scheme 1-Stage III. When KI aqueous solution was replaced by KCl aqueous solution, the upper green n-hexane dispersion would turn indigo and then blue-purple. This process takes 32 h or even more. In addition, when KI aqueous solution was substituted with KBr aqueous solution, the color of the upper green n-hexane dispersion remained unchanged. Moreover, slightly disturbing the mixing solution during this process would increase the anion exchange rate. The KX can be substituted by other metal halides, such as NaX, ZnX₂, CuX₂, MgX₂, and CaX₂, the color change of the mixture is almost as the same as KX, while the reaction time is variable depending on the halide source.



Scheme 1. Schematic diagram of synthesizing CsPbX₃ (X = Cl, Br, and I) by an interfacial anion exchange reaction. Stage I shows the color of Cs₄PbBr₆ solution before KX added; Stage II shows the color of Cs₄PbBr₆ solution changed to green within several seconds when KX was added; Stage III shows the color of Cs₄PbBr₆ solution changed to red when KI was added for 24 h and changed to blue-purple when KCl was added for 32 h, respectively.

2.5. Fabrication of WLEDs Devices

To obtain highly efficient WLEDs, a blue GaN chip with a rough structure was applied [20]. The WLEDs devices consist of a CsPbBr₃ NC film, a CdSe NC film, and a blue GaN chip. To fabricate green CsPbBr₃ NCs film, the as-synthesized CsPbBr₃ NCs were dispersed into a PMMA/n-hexane solution and the mixture was vigorously stirred with a vacuum homogenizer for 6 min to degas. After

that, the mixture was injected into a mold and heated at 60 °C for 2 h to remove n-hexane. The CdSe film was prepared by adding red CdSe NCs into the silicone gel (OE-6650 A and B) and vigorously stirring with a vacuum homogenizer for 12 min to degas. Then, the mixture was injected into a mold and solidified in a vacuum oven at 80 °C for 30 min and at 150 °C for 2 h, sequentially. Finally, the green and red film layers were orderly coated on the surface of a blue GaN chip.

2.6. Characterizations

The crystal phase and surface morphology of the samples were characterized by transmission electron microscopy (TEM, JEM-2100F, JEOL, Tokyo, Japan) with an accelerating voltage of 200 kV. The phase of the as-prepared perovskite NCs were measured using an X-ray diffractometer (XRD, D8-Advance, Bruker, Germany) with a Cu-K α radiation source ($\lambda = 0.15418$ nm) at a counting rate of 2° per minute in the scanning angle (2θ) range from 5° to 50°. The ultraviolet-visible (UV-vis) absorption spectra of the samples were tested using a UV-vis spectrometer (Shimadzu, Kyoto, Japan) over the wavelength range from 300 nm to 700 nm, at 1 nm intervals. The photoluminescence (PL) spectra of the products were recorded using a fluorescence spectrophotometer (RF-6000, Shimadzu, Kyoto, Japan) with a Xe lamp as an excitation source.

3. Results and Discussion

The surface morphology of the as-synthesized Cs₄PbBr₆ NCs was characterized by TEM, as shown in Figure 1a. The TEM image demonstrates that the Cs₄PbBr₆ NCs have a diamond-like shape and show good dispersion. Figure 1b indicates that Cs₄PbBr₆ NCs have a relatively wide particle size distribution and their average size is 23.6 nm. To determine the phase structure, XRD was applied to measure the as-synthesized Cs₄PbBr₆ NCs. As shown in Figure 1c, the XRD patterns show that Cs₄PbBr₆ NCs can be indexed as rhombohedral phase (JCPDS card No. 73-2478). In addition, no other phases were observed, suggesting a high sample purity.

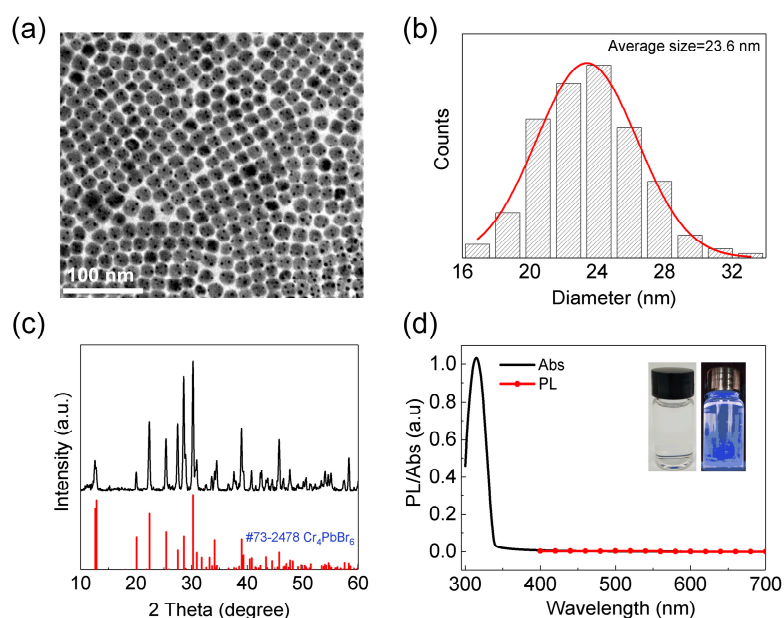


Figure 1. Characterization of Cs₄PbBr₆ nanocrystals (NCs): (a) TEM image, (b) particle size distribution, (c) X-ray diffractometer (XRD) pattern, and (d) UV-vis absorption and photoluminescence (PL) spectra. Insets are the photographs of Cs₄PbBr₆ NCs under sunlight and UV light irradiation.

The UV-vis absorption spectra and PL emission spectra of the original Cs₄PbBr₆ NCs are shown in Figure 1d. The UV-vis absorption spectrum has a single and spiculate absorption peak at 319 nm. This absorption feature is consistent with that of bulk Cs₄PbBr₆, which has been confirmed to be the

localized $6s_{1/2}$ - $6p_{1/2}$ transition within the isolated $[\text{PbBr}_6]^{4-}$ octahedra separated by Cs^+ ions [21,22]. No PL emission was observed for Cs_4PbBr_6 NCs. According to previous reports, the purified Cs_4PbBr_6 NCs did not show obvious PL emission over the entire visible range owing to their large bandgap ($E_g = 3.94$ eV) [23–25], suggesting the as-prepared Cs_4PbBr_6 NCs in this work are highly purified.

TEM was applied to characterize the three typical products obtained by interfacial anion exchange reactions. Figure 2a shows the TEM image of samples by adding KCl aqueous solution into Cs_4PbBr_6 n-hexane solution, demonstrating the samples have a regular cuboid shape with the average width of ca. 13 nm and length of ca. 32 nm, as shown in Figure S1a, b. When KCl was substituted with KBr or KI, the shape of products was almost the same as KCl, while the size and high-aspect-ratio are different, as shown in Figure 2b,c. For example, when the samples were directly obtained by Cs_4PbBr_6 transformation with KBr aqueous solution, the average width and length were 15 nm and 45 nm, respectively, and the high-aspect-ratio was 3. For the samples were synthesized by Cs_4PbBr_6 transformation with KI aqueous solution, the average width and length were 22 nm and 50 nm, respectively, and the high-aspect-ratio was 2.27. According to previous studies, this phenomenon is believed to be due to the self-assembly phenomenon of water on the formation of perovskite crystals [26–28]. This provides a new opportunity to directly synthesize crystals with different morphologies of other components. To determine the phase structure, XRD and high-angle annular dark field scanning TEM (HAADF-STEM) were used to characterize the as-prepared samples. The element mapping of HAADF-STEM in Figure S2 confirmed that the samples prepared by adding KCl into Cs_4PbBr_6 n-hexane solution were $\text{CsPbBr}_1\text{Cl}_2$. In addition, XRD patterns (Figure S3) indicated that the samples prepared using KBr and KI are CsPbBr_3 and CsPbI_3 , respectively.

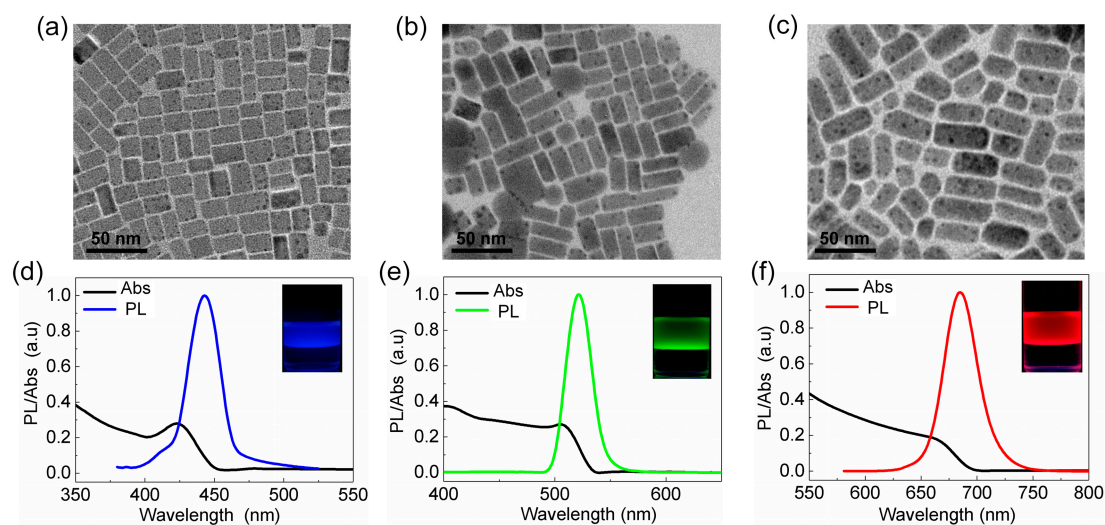


Figure 2. TEM images of samples prepared by Cs_4PbBr_6 n-hexane dispersion reaction with 0.5 mmol/mL KX (X = Cl, Br, I) aqueous solution: (a) KCl aqueous solution, (b) KBr aqueous solution, (c) KI aqueous solution. UV-vis absorption spectra and PL emission spectra of samples prepared by Cs_4PbBr_6 n-hexane dispersion reaction with 0.5 mmol/mL KX (X = Cl, Br, I) aqueous solution: (d) KCl aqueous solution, (e) KBr aqueous solution, (f) KI aqueous solution. The insets are digital photos of the products under UV light irradiation.

The UV-vis absorption and PL spectra of the corresponding samples are illustrated in Figure 2d,f. The $\text{CsPbBr}_1\text{Cl}_2$ NCs show a sharp first characteristic absorption at 427 nm and a strong PL emission peak at 435 nm with a full width at half maximum (FWHM) of 22 nm, as presented in Figure 2d. Furthermore, the small Stokes shift (8 nm) indicates the PL emission of $\text{CsPbBr}_1\text{Cl}_2$ NCs results from the bound exciton recombination [29]. In addition, the UV-vis absorption spectra and PL emission spectra of CsPbBr_3 NCs show the first characteristic absorption peak of approximately 508 nm and the PL emission of around 520 nm with a narrow FWHM of 18 nm, and the UV-vis absorption peak

and PL emission peak of CsPbI₃ NCs were 670 nm and 690 nm, respectively. The PL QY of the as-prepared CsPbBr₁Cl₂ NCs, CsPbBr₃ NCs and CsPbI₃ NCs were measured to be ca. 45%, 80%, and 68% (Rhodamin 101 as reference, PL QY is 100%), respectively [30,31]. The insets in Figure 2d–f are representative digital pictures of each sample under 365 nm UV light irradiation, showing bright blue, green, and red fluorescence and indicating samples with high PL QY were formed. The above results clearly confirmed that the interfacial anion exchange processes were successfully completed for synthesizing different component products.

To observe the spectral shift of these anion-exchange reactions in situ, representative UV-vis absorption spectra and PL spectra of such exchanged CsPbX₃ NCs, are shown in Figure 3. By adding KCl into Cs₄PbBr₆ n-hexane solution, the first characteristic absorption peak of as-prepared samples gradually blue-shifted and finally reached 420 nm. This gradual shift is consistent with the XRD result due to the substitution of Br[−] with Cl[−]. When KCl was substituted with KI, the absorption peak gradually red-shifted and finally reached 675 nm. In addition, we observed that the first characteristic absorption spectra gradually became sharper when adding KCl and became broader when adding KI over time, which is similar to a previously reported study [19]. The PL spectra of the CsPbX₃ NCs that transformed from Cs₄PbBr₆ NCs are Stokes-shifted with respect to the optical absorption, as shown in Figure 3b,c. According to the interfacial ion exchange process, the UV-vis absorption and PL spectra matched well with those of the directly synthesized CsPbX₃ NCs in previous reports [32], indicating that the CsPbX₃ can be easily obtained by anion exchange in the interface of an n-hexane and KX aqueous solution.

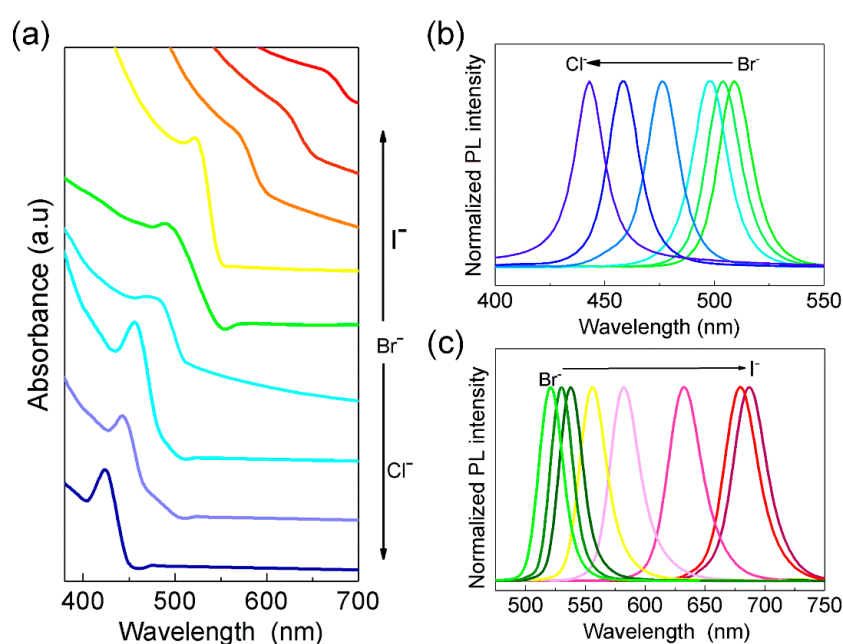


Figure 3. (a) Evolution of the UV-vis absorption spectra of samples that were prepared by the Cs₄PbBr₆ n-hexane dispersion reaction with 0.5 mmol/mL KX (X = Cl, Br, and I) aqueous solution. (b) PL spectra of the exchanged NCs obtained from the Cs₄PbBr₆ n-hexane dispersion by using (b) KCl and (c) KI aqueous solution as anion exchange resources.

The concentration of KX plays an important role in the spectral shift during the anion exchange process. To study the effect of concentration of KX aqueous on optical properties of as-prepared samples, a series of KX aqueous concentrations control experiments have been conducted. During the interfacial anion exchange process, some aliquots of the reaction mixture were removed from the reaction system, and the samples were characterized by PL spectrometry. Figure 4a,b show the emission peak position and PL emission energy as a function of time after adding different concentrations of KCl solution into the Cs₄PbBr₆ n-hexane solution. When the concentration of KCl was 0.2 M, the PL

emission peak increased from 520 nm to 425 nm over time, and the corresponding PL emission energy increased from 2.38 eV to 2.88 eV. As the concentration of KCl increased, the rate of blue-shift increased. This is because the increase of ion concentration results in the increase of the frequency of ion contact, which leads to the acceleration of the exchange rate. When KI was added to the Cs_4PbBr_6 n-hexane solution, the PL emission peak shifted from 520 nm to 650 nm with a displacement of 130 nm, and the corresponding emission energy decreased from 2.38 eV to 1.90 eV (Figure 4c,d). Increasing the concentration of KX will improve the exchange rate, but the ultimate limit of movement is almost the same.

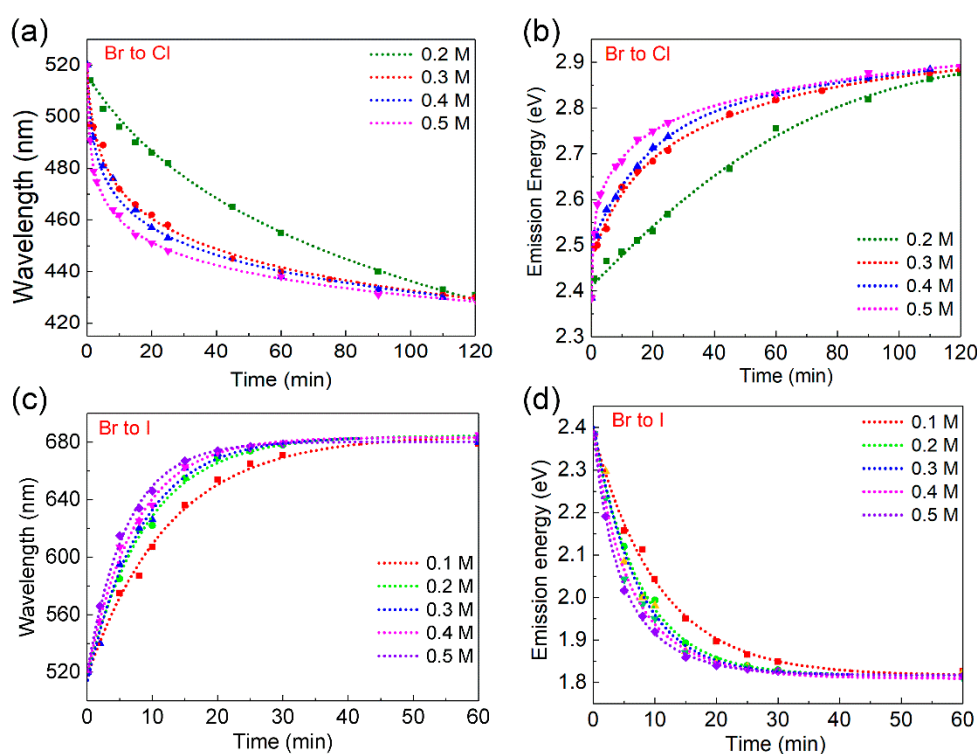


Figure 4. (a) PL wavelength and (b) emission peak energies of samples that were prepared by the Cs_4PbBr_6 n-hexane dispersion reaction with various concentrations (0.2 M ~ 0.5 M) of KCl aqueous solution. (c) PL wavelength and (d) emission peak energies of samples that were prepared by the Cs_4PbBr_6 n-hexane dispersion reaction with various concentrations (0.1 M ~ 0.5 M) of KI aqueous solution.

Furthermore, this process could be repeated when KX was replaced by other halide sources, such as NaX and ZnX_2 , as demonstrated in Figures S4 and S5. The change in the PL spectra of the samples that were synthesized by Cs_4PbBr_6 transformation with ZnX_2 solutions, as shown in Figure S4a–b, suggested the Cs_4PbBr_6 successfully transformed to CsPbX_3 in these solutions and realized the spectral shift. For different metal halides, the reaction time of interfacial anion exchange reaction and the wavelength range for the PL emission spectra are different. This phenomenon is thought to be caused by the influence of different metal cations on the diffusion of halogen ions at the interface.

To detailed explore the process of interfacial anion exchange, TEM and XRD were applied to monitor the change on the morphology and size of typical $\text{CsPbBr}_x\text{I}_{3-x}$ NCs. Figure 5a shows the representative TEM images of Cs_4PbBr_6 NCs after 0, 4, 8, and 24 h when KI was added, respectively. At 4 h, the TEM image shows a mainly regular cuboid shape with a small portion of diamond-like shape, indicating the interfacial anion exchange reaction occurred. As storage time was extended, well-defined, and mono-dispersed, CsPbI_3 NCs were achieved and their size increased significantly. The XRD pattern of the samples is depicted in Figure 5b. The diffraction peaks of the Cs_4PbBr_6 NCs were indexed as rhombohedral phase (JCPDS card No. 73-2478), and no other peaks were observed.

When the original Cs_4PbBr_6 n-hexane reacted with the KI aqueous solution for only 4 h, main diffraction peaks at $2\theta = 13.1^\circ, 17.6^\circ, 25.7^\circ, 27.4^\circ, 30.4^\circ, 35.3^\circ, 37.7^\circ,$ and 44.4° were detected, indicating that the $\text{CsPbBr}_x\text{I}_{3-x}$ NCs were formed. Significantly, the peaks at $2\theta = 15.2^\circ, 21.6^\circ, 26.5^\circ, 30.6^\circ, 34.4^\circ, 37.8^\circ,$ and 43.9° were observed, indicating that CsPbBr_3 NCs were synthesized. Upon the addition of KI solution, due to the high solubility of CsBr in water solution (1243 g/L at 25°C) [33], the decomposition of Cs_4PbBr_6 and the formation of CsPbBr_3 NCs was driven. This is consistent with the phenomenon where the mixture turned green immediately after the KX solution was added into the Cs_4PbBr_6 n-hexane solution. Moreover, it is worth mentioning that no broad peaks at $2\theta = 20\text{--}25^\circ$ (a characteristic feature of amorphous materials) have been detected, which can be ascribed to the high crystallinity of Cs_4PbBr_6 and CsPbBr_3 NCs. These results confirmed that at the KX aqueous solution interface, the driving force of water will first convert Cs_4PbBr_6 into CsPbBr_3 , while the halogen ion does not directly react with Cs_4PbBr_6 but with CsPbBr_3 .

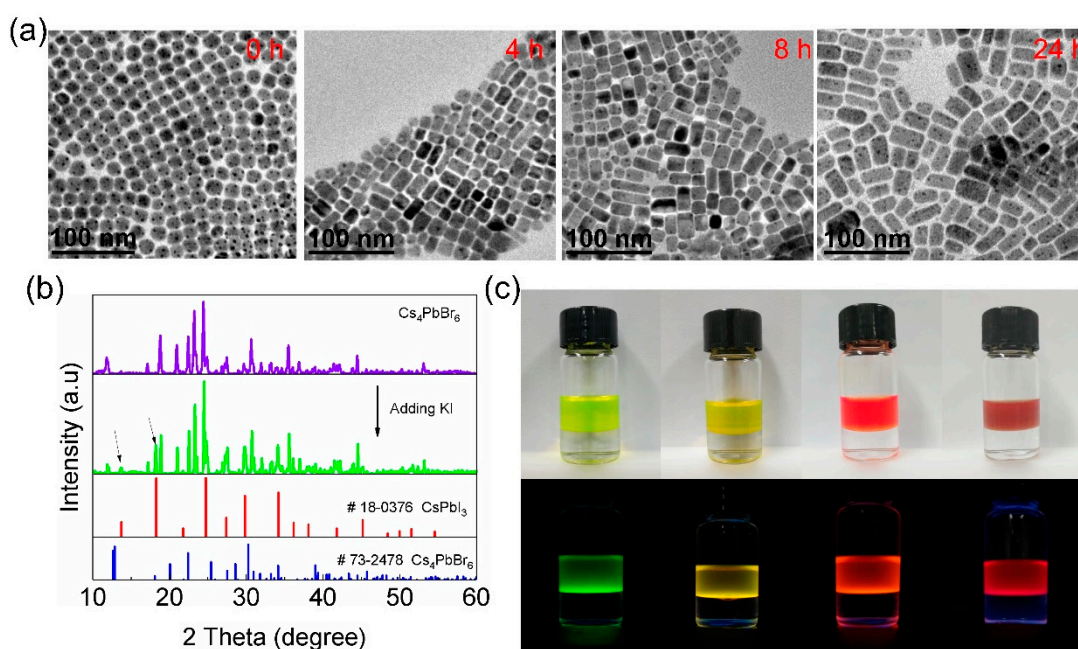


Figure 5. (a) Time-dependent TEM image of the product obtained by Cs_4PbBr_6 NCs reacting with KI aqueous solution. (b) XRD pattern of the final product of KI aqueous solution reaction. (c) Digital photos of the system under sunlight and UV light.

The corresponding digital photos of four typical samples are shown in Figure 5c. When KI was added, the original transparent Cs_4PbBr_6 n-hexane solution divided into two layers immediately and showed a light green-yellow color in the top layer. With the time prolonged, the green-yellow color became yellow and red gradually, implying the interfacial anion exchange reaction between Br^- and I^- occurred. When the as-prepared products were irradiated with UV light, a bright photoluminescence was observed. Significantly, as the anion exchange reaction completed, the color of the sample synthesized by this method showed a much higher stability. After being stored for 48 h, the sample underwent UV light irradiation, the red solution kept almost the same color and no clear decay in photoluminescence was detected, implying high stability against moisture.

Through the above-mentioned analysis, a possible mechanism was proposed, as illustrated in Figure 6. The original material Cs_4PbBr_6 NCs were dispersed in n-hexane and their surface coated with the oleic acid and oleylamine, which resulted in hydrophobicity to ensure the stable presence of NCs in non-polar solvents. After adding KX aqueous solution, CsBr was stripped through the n-hexane/water interface due to its high solubility and the non-fluorescent Cs_4PbBr_6 NCs were converted to green fluorescent CsPbBr_3 NCs. Meanwhile, oleic acid and oleylamine on the NCs surface are highly

dynamic due to the water-driven mechanism, which makes the conversion process more accessible. It is well-known that KX has very low solubility in n-hexane but its solubility in water is very high and it would be quickly ionized into halogen ions in water. Therefore, the halogen anions in the aqueous phase have an excellent diffusion capacity at the n-hexane/water interface. When KX solution was added to Cs_4PbBr_6 NCs n-hexane solution, ionized halogen ions slowly diffused into the n-hexane and reacted with as-synthesized CsPbBr_3 NCs causing the optical spectrum redshift or blueshift. Since the halogen ions diffusing near the n-hexane interface are consumed after the reaction, the diffusion behavior of the anions can be continuously performed without external energy input. Notably, the solubility of KX in n-hexane is extremely low; thus, only a small part of the K^+ ion in the aqueous phase can enter n-hexane. This ensures the “pure” in that the anion exchange process does not create other non-luminescent substances. Additionally, when this system encounters slight stirring after adding KX aqueous solution, the rate of interface anion exchange can be accelerated.

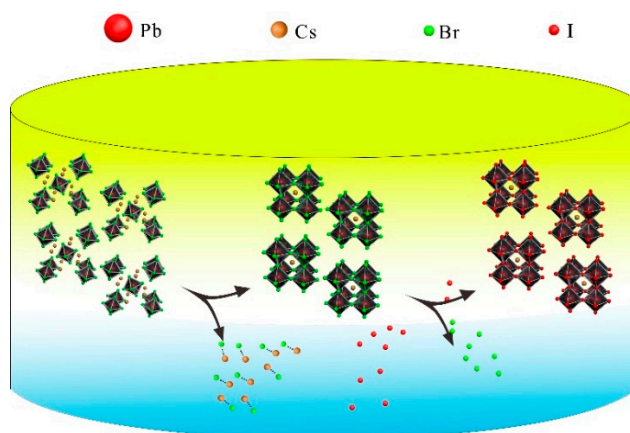


Figure 6. Illustration of the mechanism for the synthesis of CsPbX_3 perovskite NCs by interfacial anion exchange reaction.

Perovskite NCs or other quantum dots are generally unstable at high temperatures [34]. Considering such thermal instability of the perovskite NCs and the heat generated by blue LED chips, an effective approach to avoid the temperature effect is to use the remote phosphor configuration, in which the phosphor layer is separated from the LED excitation light source [35,36]. To evaluate the as-synthesized CsPbX_3 NCs for white LED (WLED) applications, the WLEDs, including green CsPbBr_3 NCs film, a red CdSe film, and a blue LED chip, were fabricated. The electroluminescence (EL) spectra of Figure 7a revealed that the CsPbBr_3 NCs have a narrow EL bandwidth, which coincides with the white light requirement of backlight displays. The International Commission on Illumination (CIE) chromaticity coordinates in Figure 7b shows that the WLEDs device presents cold white light (CCT is at approximately 6,300 and (x, y) is at around (0.32, 0.34), respectively) at different currents. Moreover, the WLEDs device shows an encompassing 125% color gamut of the National Television System Committee (NTSC, 1913) standard. This result indicates that the device could be useful as a next-generation candidate for high-end professional displays. The EL spectra of the WLEDs at different driving currents are shown in Figure 7c. The spectral intensity increased as current from 50 to 600 mA and the spectral shape remained almost unchanged, indicating that the CsPbBr_3 NCs were not saturated by blue light. The luminous efficiency and flux of the WLEDs were determined, as shown in Figure 7d. The highest luminous efficiency was 32.7 lm/W, which is much higher than most perovskite quantum dot LEDs (Table S1).

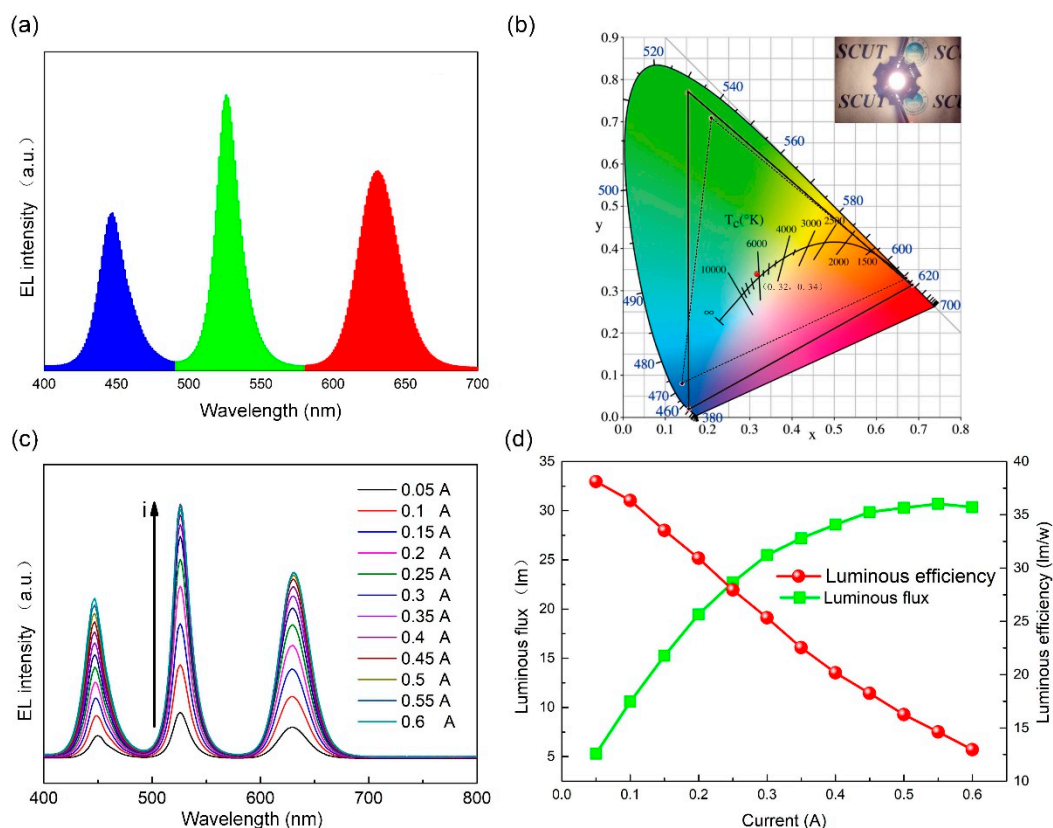


Figure 7. (a) Electroluminescence (EL) spectra of the white LED (WLED) device based on transformed CsPbBr₃ NCs. (b) The International Commission on Illumination (CIE) color diagram of the WLED device and the color gamut of blue LED, green CsPbBr₃ NCs, red CdSe NCs (solid line), and NTSC standard (dashed line). The labeled red point in (c) is the color coordinate of the CsPbBr₃-based device. Inset shows a photograph of the device operating at a forward current of 100 mA. (c) Current-dependent EL spectra. (d) Luminous flux and luminous efficiency of WLEDs at different forward currents.

4. Conclusions

In summary, we reported a facile and environmentally friendly method for the synthesis of highly stable and photoluminescent CsPbX₃ through interfacial anion exchange reaction. By adding KX aqueous solution, we enabled the efficient chemical transformation of non-luminescent Cs₄PbBr₆ NCs to highly photoluminescent CsPbX₃ NCs. The spectral shift of CsPbX₃ NCs under different metal halide concentrations and sources were also investigated. By using different metal halides, the bandgap energy and PL spectra of CsPbX₃ NCs were readily tuned over the entire visible spectral region. In addition, a chemical transformation mechanism between Cs₄PbBr₆ NCs and CsPbX₃ NCs was investigated. The mechanism revealed that Cs₄PbBr₆ NCs dispersed in n-hexane were converted to CsPbBr₃ NCs first by stripping CsBr through an interfacial reaction with aqueous solution. This process takes advantage of the high solubility of CsBr in KX aqueous solution, producing air-stable CsPbBr₃ NCs, and then the CsPbBr₃ NCs exchange with halogen ions at the interface of n-hexane/water. The interfacial anion exchange method eliminates the dependence of halogen ionic solubility on oleic acid and oleylamine. Moreover, water and n-hexane separated perovskite NCs from halogenated inorganic salts at the interface, so that non-luminescent substances could not enter into the CsPbX₃ NCs in large quantities, ensuring their purity. WLEDs device were fabricated by combining the green luminescent CsPbBr₃ NCs with red luminescent CdSe NCs and a blue GaN LED chip, obtaining a high color gamut of 125% (NTSC standard). There is still a need to obtain pure and highly stable CsPbX₃ NCs, especially for CsPbCl₃ NCs.

Supplementary Materials: The following are available online at <http://www.mdpi.com/2079-4991/9/9/1296/s1>, Figure S1a,b. The statistics of width and length of the samples when KCl was added. Figure S1c,d. The statistics of width and length of the samples when KBr was added. Figure S1e,f. The statistics of width and length of the samples when KI was added. Figure S2: Element mapping of the samples prepared by Cs₄PbBr₆ transformation with KCl aqueous solution, Figure S3: XRD patterns of the samples prepared by Cs₄PbBr₆ transformation with (a) KBr and (b) KI aqueous solution, Figure S4: The PL spectra of the samples that were synthesized by Cs₄PbBr₆ transformation with different halide solutions (a) ZnCl₂, (b) ZnI₂, (c) NaCl, and (d) NaI, Figure S5. The color change of the samples that were synthesized by the Cs₄PbBr₆ transformation with different concentrations of (a) ZnCl₂ and (b) ZnI₂ aqueous solution. Table S1. The luminous efficiency of different types of perovskite light emitting-diodes.

Author Contributions: Conceptualization, L.R. and Z.L.; methodology, L.R., C.S., and H.L.; software, K.C., C.Y., and H.L.; validation, X.D. and Z.L.; formal analysis, L.R., C.Y., and Z.L.; investigation, H.L., C.Y., and K.C.; resources, Y.T. and Z.L.; data curation, C.S.; writing—original draft preparation, Z.L., C.S., and L.R.; writing—review and editing, L.R., C.S., Z.L., and Y.T.; visualization, Z.L. and L.R.; supervision, X.D., Z.L., and B.Y.; project administration, Y.T., X.D., B.Y., and Z.L.; funding acquisition, Z.L., B.Y., and Y.T.

Funding: This work was supported by National Natural Science Foundation of China (51775199, 51735004), Natural Science Foundation of Guangdong Province (2018B030306008), and the Science & Technology Program of Guangdong Province (2017B010115001).

Conflicts of Interest: The authors declare no conflict of interest.

References

1. He, X.; Qiu, Y.; Yang, S. Fully-inorganic trihalide perovskite nanocrystals: A new research frontier of optoelectronic materials. *Adv. Mater.* **2017**, *29*, 1700775. [[CrossRef](#)] [[PubMed](#)]
2. Huang, H.; Bodnarchuk, M.I.; Kershaw, S.V.; Kovalenko, M.V.; Rogach, A.L. Lead halide perovskite nanocrystals in the research spotlight: Stability and defect tolerance. *ACS Energy Lett.* **2017**, *2*, 2071–2083. [[CrossRef](#)] [[PubMed](#)]
3. Rao, L.; Tang, Y.; Song, C.; Xu, K.; Vickers, E.T.; Bonabi Naghadeh, S.; Ding, X.; Li, Z.; Zhang, J.Z. Polar-solvent-free synthesis of highly photoluminescent and stable CsPbBr₃ nanocrystals with controlled shape and size by ultrasonication. *Chem. Mater.* **2018**, *31*, 365–375. [[CrossRef](#)]
4. Swarnkar, A.; Chulliyil, R.; Ravi, V.K.; Irfanullah, M.; Chowdhury, A.; Nag, A. Colloidal CsPbBr₃ perovskite nanocrystals: Luminescence beyond traditional quantum dots. *Angew. Chem. Int. Ed.* **2015**, *54*, 15424–15428. [[CrossRef](#)] [[PubMed](#)]
5. Chang, X.; Li, W.; Zhu, L.; Liu, H.; Geng, H.; Xiang, S.; Liu, J.; Chen, H. Carbon-based CsPbBr₃ perovskite solar cells: All-ambient processes and high thermal stability. *ACS Appl. Mater. Interfaces* **2016**, *8*, 33649–33655. [[CrossRef](#)]
6. Park, K.; Lee, J.W.; Kim, J.D.; Han, N.S.; Jang, D.M.; Jeong, S.; Park, J.; Song, J.K. Light-matter interactions in cesium lead halide perovskite nanowire lasers. *J. Phys. Chem. Lett.* **2016**, *7*, 3703–3710. [[CrossRef](#)] [[PubMed](#)]
7. Song, X.; Liu, X.; Yu, D.; Huo, C.; Ji, J.; Li, X.; Zhang, S.; Zou, Y.; Zhu, G.; Wang, Y. Boosting two-dimensional MoS₂/CsPbBr₃ photodetectors via enhanced light absorbance and interfacial carrier separation. *ACS Appl. Mater. Interfaces* **2018**, *10*, 2801–2809. [[CrossRef](#)]
8. Rao, L.; Tang, Y.; Yan, C.; Li, J.; Zhong, G.; Tang, K.; Yu, B.; Li, Z.; Zhang, J.Z. Tuning the emission spectrum of highly stable cesium lead halide perovskite nanocrystals through poly (lactic acid)-assisted anion-exchange reactions. *J. Mater. Chem. C* **2018**, *6*, 5375–5383. [[CrossRef](#)]
9. Protesescu, L.; Yakunin, S.; Bodnarchuk, M.I.; Krieg, F.; Caputo, R.; Hendon, C.H.; Yang, R.X.; Walsh, A.; Kovalenko, M.V. Nanocrystals of cesium lead halide perovskites (CsPbX₃, X = Cl, Br, and I): Novel optoelectronic materials showing bright emission with wide color gamut. *Nano Lett.* **2015**, *15*, 3692–3696. [[CrossRef](#)]
10. Li, G.; Wang, H.; Zhang, T.; Mi, L.; Zhang, Y.; Zhang, Z.; Zhang, W.; Jiang, Y. Solvent-polarity-engineered controllable synthesis of highly fluorescent cesium lead halide perovskite quantum dots and their use in white light-emitting diodes. *Adv. Funct. Mater.* **2016**, *26*, 8478–8486. [[CrossRef](#)]
11. Zhang, W.; Eperon, G.E.; Snaith, H.J. Metal halide perovskites for energy applications. *Nat. Energy* **2016**, *1*, 16048. [[CrossRef](#)]

12. Tong, Y.; Bladt, E.; Aygüler, M.F.; Manzi, A.; Milowska, K.Z.; Hintermayr, V.A.; Docampo, P.; Bals, S.; Urban, A.S.; Polavarapu, L. Highly luminescent cesium lead halide perovskite nanocrystals with tunable composition and thickness by ultrasonication. *Angew. Chem. Int. Ed.* **2016**, *55*, 13887–13892. [[CrossRef](#)] [[PubMed](#)]
13. Jana, A.; Mittal, M.; Singla, A.; Sapra, S. Solvent-free, mechanochemical syntheses of bulk trihalide perovskites and their nanoparticles. *Chem. Commun.* **2017**, *53*, 3046–3049. [[CrossRef](#)] [[PubMed](#)]
14. Protesescu, L.; Yakunin, S.; Nazarenko, O.; Dirin, D.; Kovalenko, M. Low-cost synthesis of highly luminescent colloidal lead halide perovskite nanocrystals by wet ball milling. *ACS Appl. Nano Mater.* **2018**, *1*, 1300–1308. [[CrossRef](#)] [[PubMed](#)]
15. Zhang, D.; Eaton, S.W.; Yu, Y.; Dou, L.; Yang, P. Solution-phase synthesis of cesium lead halide perovskite nanowires. *J. Am. Chem. Soc.* **2015**, *137*, 9230–9233. [[CrossRef](#)] [[PubMed](#)]
16. Zhou, H.; Yuan, S.; Wang, X.; Xu, T.; Wang, X.; Li, H.; Zheng, W.; Fan, P.; Li, Y.; Sun, L. Vapor growth and tunable lasing of band gap engineered cesium lead halide perovskite micro/nanorods with triangular cross section. *ACS Nano* **2016**, *11*, 1189–1195. [[CrossRef](#)]
17. Akkerman, Q.A.; Park, S.; Radicchi, E.; Nunzi, F.; Mosconi, E.; De Angelis, F.; Brescia, R.; Rastogi, P.; Prato, M.; Manna, L. Nearly monodisperse insulator Cs₄PbX₆ (X = Cl, Br, I) nanocrystals, their mixed halide compositions, and their transformation into CsPbX₃ nanocrystals. *Nano Lett.* **2017**, *17*, 1924–1930. [[CrossRef](#)]
18. Jing, Q.; Su, Y.; Xing, X.; Lu, Z. Highly luminescent CsPbBr₃ nanorods synthesized by a ligand-regulated reaction at the water-oil interface. *J. Mater. Chem. C* **2019**, *7*, 1854–1858. [[CrossRef](#)]
19. Nedelcu, G.; Protesescu, L.; Yakunin, S.; Bodnarchuk, M.I.; Grotevent, M.J.; Kovalenko, M.V. Fast anion-exchange in highly luminescent nanocrystals of cesium lead halide perovskites (CsPbX₃, X = Cl, Br, I). *Nano Lett.* **2015**, *15*, 5635–5640. [[CrossRef](#)]
20. Li, Z.; Cao, K.; Li, J.; Tang, Y.; Xu, L.; Ding, X.; Yu, B. Investigation of light-extraction mechanisms of multiscale patterned arrays with rough morphology for gan-based thin-film LEDs. *IEEE Access* **2019**, *7*, 73890–73898. [[CrossRef](#)]
21. Rao, L.; Ding, X.; Du, X.; Liang, G.; Tang, Y.; Tang, K.; Zhang, J.Z. Ultrasonication-assisted synthesis of CsPbBr₃ and Cs₄PbBr₆ perovskite nanocrystals and their reversible transformation. *Beilstein J. Nanotech.* **2019**, *10*, 666–676. [[CrossRef](#)] [[PubMed](#)]
22. Liu, Z.; Bekenstein, Y.; Ye, X.; Nguyen, S.C.; Swabeck, J.; Zhang, D.; Lee, S.-T.; Yang, P.; Ma, W.; Alivisatos, A.P. Ligand mediated transformation of cesium lead bromide perovskite nanocrystals to lead depleted Cs₄PbBr₆ nanocrystals. *J. Am. Chem. Soc.* **2017**, *139*, 5309–5312. [[CrossRef](#)] [[PubMed](#)]
23. Yin, J.; Zhang, Y.; Bruno, A.; Soci, C.; Bakr, O.M.; Brédas, J.-L.; Mohammed, O.F. Intrinsic lead ion emissions in zero-dimensional Cs₄PbBr₆ Nanocrystals. *ACS Energy Lett.* **2017**, *2*, 2805–2811. [[CrossRef](#)]
24. Zhang, Y.; Saidaminov, M.I.; Dursun, I.; Yang, H.; Murali, B.; Alarousu, E.; Yengel, E.; Alshankiti, B.A.; Bakr, O.M.; Mohammed, O.F. Zero-dimensional Cs₄PbBr₆ perovskite nanocrystals. *J. Phys. Chem. Lett.* **2017**, *8*, 961–965. [[CrossRef](#)] [[PubMed](#)]
25. Akkerman, Q.A.; Abdelhady, A.L.; Manna, L. Zero-dimensional cesium lead halides: History, properties, and challenges. *J. Phys. Chem. Lett.* **2018**, *9*, 2326–2337. [[CrossRef](#)] [[PubMed](#)]
26. Zhang, X.; Bai, X.; Wu, H.; Zhang, X.; Sun, C.; Zhang, Y.; Zhang, W.; Zheng, W.; Yu, W.W.; Rogach, A.L. Water-assisted size and shape control of CsPbBr₃ perovskite nanocrystals. *Angew. Chem. Int. Ed.* **2018**, *57*, 3337–3342. [[CrossRef](#)] [[PubMed](#)]
27. Pushkarev, A.P.; Korolev, V.I.; Markina, D.I.; Komissarenko, F.E.; Naujokaitis, A.; Drabavičius, A.; Pakštas, V.; Franckevičius, M.; Khubezhov, S.A.; Sannikov, D.A. A few-minute synthesis of CsPbBr₃ nanolasers with a high quality factor by spraying at ambient conditions. *ACS Appl. Mater. Interfaces* **2018**, *11*, 1040–1048. [[CrossRef](#)] [[PubMed](#)]
28. Turedi, B.; Lee, K.J.; Dursun, I.; Alamer, B.; Wu, Z.; Alarousu, E.; Mohammed, O.F.; Cho, N.; Bakr, O.M. Water-induced dimensionality reduction in metal-halide perovskites. *J. Phys. Chem. C* **2018**, *122*, 14128–14134. [[CrossRef](#)]
29. Liang, Z.; Zhao, S.; Xu, Z.; Qiao, B.; Song, P.; Gao, D.; Xu, X. Shape-controlled synthesis of all-inorganic CsPbBr₃ perovskite nanocrystals with bright blue emission. *ACS Appl. Mater. Interfaces* **2016**, *8*, 28824–28830. [[CrossRef](#)]
30. Brouwer, A.M. Standards for photoluminescence quantum yield measurements in solution (IUPAC Technical Report). *Pure Appl. Chem.* **2011**, *83*, 2213–2228. [[CrossRef](#)]

31. Ishida, H.; Bünzli, J.; Beeby, A. Guidelines for measurement of luminescence spectra and quantum yields of inorganic and organometallic compounds in solution and solid state (IUPAC Technical Report). *Pure Appl. Chem.* **2016**, *88*, 701–711. [[CrossRef](#)]
32. Li, X.; Wu, Y.; Zhang, S.; Cai, B.; Gu, Y.; Song, J.; Zeng, H. CsPbX₃ quantum dots for lighting and displays: Room-temperature synthesis, photoluminescence superiorities, underlying origins and white light-emitting diodes. *Adv. Funct. Mater.* **2016**, *26*, 2435–2445. [[CrossRef](#)]
33. Wu, L.; Hu, H.; Xu, Y.; Jiang, S.; Chen, M.; Zhong, Q.; Yang, D.; Liu, Q.; Zhao, Y.; Sun, B. From nonluminescent Cs₄PbX₆ (X = Cl, Br, I) nanocrystals to highly luminescent CsPbX₃ nanocrystals: Water-triggered transformation through a CsX-stripping mechanism. *Nano Lett.* **2017**, *17*, 5799–5804. [[CrossRef](#)] [[PubMed](#)]
34. Li, Z.; Song, C.; Qiu, Z.; Li, J.; Cao, K.; Ding, X.; Tang, Y. Study on the thermal and optical performance of quantum dot white light-emitting diodes using metal-based inverted packaging structure. *IEEE Trans. Electron Devices* **2019**, *66*, 3020–3027. [[CrossRef](#)]
35. Li, J.; Tang, Y.; Li, Z.; Ding, X.; Rao, L.; Yu, B. Effect of quantum dot scattering and absorption on the optical performance of white light-emitting diodes. *IEEE Trans. Electron Devices* **2018**, *65*, 2877–2884. [[CrossRef](#)]
36. Tang, Y.; Lu, H.; Li, J.; Li, Z.; Du, X.; Ding, X.; Yu, B. Improvement of optical and thermal properties for quantum dots WLEDs by controlling layer location. *IEEE Access* **2019**, *7*, 77642–77648. [[CrossRef](#)]



© 2019 by the authors. Licensee MDPI, Basel, Switzerland. This article is an open access article distributed under the terms and conditions of the Creative Commons Attribution (CC BY) license (<http://creativecommons.org/licenses/by/4.0/>).